Journal of Magnetism and Magnetic Materials 95 (1991) 123–132
North-Holland



# Surface chemical state of sputtered Co–Cr films

T. Masuda, W.J.M.A. Geerts and J.C. Lodder

*Information Storage Technology Group, Faculty of Electric Engineering, University of Twente, P.O. Box 217, 7500 AE Enschede, The Netherlands*

Surface oxidation states of sputtered $Co_{80}Cr_{20}$ (at%) films were studied by performing Auger Electron Spectroscopy (AES) and X-ray Photoemission Spectroscopy (XPS). Seven samples having different thicknesses (from 50 to 1000 nm) which were grown under the same conditions have been studied. It was found from these experiments that among all the films the initial oxidation occurred in the Cr; then the following diffusion of the Co was observed at the top layer. Consequently the surface consists of a four-layered structure. A weak thickness dependence in the films of the oxidized region was found from the results of AES measurements. The change of the saturation magnetization through the sample was calculated using the results of AES and XPS data. These calculations show that a region with enhanced saturation magnetization can be expected under the non-ferromagnetic top layer.

## 1. Introduction

Sputtered Co–Cr films are considered to be one of the materials showing great promise for applications as high-density perpendicular magnetic recording media [1]. Recently interest in the surface has become more important because the actual medium thickness will decrease continuously for the purpose of higher-density recording.

In order to understand the complex system of the Co–Cr medium in more detail a great deal of effort has been spent on the study of the surface magnetic behaviour [2–6]. Although much knowledge about the influence of Cr content, substrates and deposition parameters on magneto-optical parameters has been revealed, a lack of sufficient data about the chemical state of the surface makes it difficult to interpret the results [7–13].

Several studies have been performed in the past to determine the nature of the oxygen layer in Co–Cr. At the end of the 1960s, Kofstad and Hed [14–16] studied the oxidation behaviour of bulk Co–Cr at high temperatures (between 900 and 1200 °C). A duplex oxygen scale, i.e. an outer CoO layer and an inner CoO layer with inclusions of $Cr_2O_3$ and $CoCr_2O_4$, was observed. The development of cracks and pores during the annealing process is largely influenced by the oxidation kinetics. Recently Kitakami et al. [13] reported the results of lower temperature annealing experiments (up to 400 °C) on evaporated samples. Based on both AES and XPS depth profiling experiments, they proposed a triplex oxygen scale above the bulk concentration of Co–Cr: (i) CoO/(ii) CoO and $Cr_2O_3$/(iii) Co–Cr and $Cr_2O_3$.

In this paper we will discuss the results obtained by performing AES and Angle-Resolved XPS (ARXPS) analyses on the surface of sputtered Co–Cr samples. Special attention is paid to the sample thickness dependence of the oxygen scale and its possible influence on the magnetic properties.

## 2. Experimental

### 2.1. Sample preparation

All the samples were prepared by rf sputtering on single-crystal Si (100) wafers which have a thickness of (280 ± 25) μm and a diameter of 50.8 mm. The Si surface was cleaned of adsorbed layers by glow discharge ($V_{rf}$: −0.5 kV, $I$: 98 mA, $P_{Ar}$: 0.4 Pa). Seven different Co–Cr samples were de-

0304-8853/91/$03.50 

posited under the conditions of the previous report [17] ($V_{rf}$: −1.6 kV, $I$; 293 mA $P_{Ar}$: 0.4 Pa). Under the same conditions, pure Co and Cr films were also deposited in the same sputtering system, as standard samples for making comparisons with Co–Cr. The samples were stored under ordinary atmospheric conditions after deposition. They were cut to the size of $10 \times 10$ mm$^2$ for magnetic and XPS measurements and $3 \times 10$ mm$^2$ for AES measurements.

The characteristics of these samples are shown in table 1. In this table the values of *1 and *3 were determined from the results of X-ray Fluorescence (XRF) measurements. Using a Scanning Electron Microscope (SEM) the values of *2 were measured. Cr concentration in the samples was also determined by XRF and was about 19.2 at% in every sample.

The half-width angles ($\Delta\theta_{50}$) from the {0002} rocking curves were determined by X-ray diffraction (XRD) using Cu-$K_\alpha$ radiation and appeared to be within 2.5 to 4.5°.

### 2.2. Magnetic measurements

A Vibrating Sample Magnetometer (VSM) was used for analysing the magnetic character of the samples [5]. The perpendicular hysteresis curves were measured, from which we determined saturation magnetization ($M_{S(VSM)}$) and coercivity ($H_{C(VSM)}$). $M_{S(VSM)}$ appeared to be roughly constant and independent of the film thickness which is in agreement with previous work [4,5].

The perpendicular hysteresis curve of the surface was also measured with a Magneto-Optic (MO) Kerr tracer using a HeNe laser (λ: 632.8 nm) [18]. Saturation Kerr rotation ($\theta_s$) and coercivity ($H_{C(Kerr)}$) were strongly dependent on the sample thickness as shown in table 1 [6].

### 2.3. AES analyses

The AES analyses were performed with a Scanning Auger Multiprobe Model PHI-600 (Perkin–Elmer, Physical Electronics Division) equipped with a cylindrical mirror analyser having a coaxial electron gun (type 25-120A: Perkin–Elmer Physical Electronics Division). The conditions for measuring were determined experimentally from preexperiments: i.e. primary beam energy: 3 kV, beam current: 100 nA. The excitation beam area was adopted in two ways; as a scanning-mode analysis and as a point analysis; the former case was approximately 0.2 μm$^2$ and the latter $10^{-4}$ μm$^2$. The analysed beam area was large enough to compare with the columnar diameter (see table 1), therefore the results obtained from both analyses were the same. This also means that the surfaces of the samples show good homogeneity. Basic pressure was below $4 \times 10^{-8}$ Pa.

In order to clean the film surface and perform depth profiling, $Ar^+$ ion bombardment was carried out using a differentially pumped sputter ion gun (beam energy: 3.5 keV, emission current: 2.5 mA). The sputtering rate can be changed by adjusting the scanning area of the ion gun. Working pressure during sputtering was approximately $6 \times 10^{-6}$ Pa.

Auger spectra were recorded between 30 and 2000 eV with a step width of 1.0 eV.

Table 1
Properties of the sputtered samples

| Sample no. | Thickness (nm) | $D_{col}$ [a] (nm) | $d_{surf}$ [c] (nm) | $Cr_{cont}$ [b] (at%) | $H_{C\perp VSM}$ (kA/m) | $H_{C\perp Kerr}$ (kA/m) | $\theta_{s\,Kerr}$ (°) |
|---|---|---|---|---|---|---|---|
| 1 | 44 | – | 2.5 | | 79 | 90 | 0.163 |
| 2 | 80 | 57±13 | 3.0 | | 102 | 88 | 0.163 |
| 3 | 110 | – | 3.2 | | 96 | 67 | 0.163 |
| 4 | 157 | 100±25 | 3.5 | 19.2 | 88 | 40 | 0.149 |
| 5 | 297 | – | 3.8 | (average) | 65 | 9 | 0.123 |
| 6 | 611 | 125±33 | 3.8 | | 46 | 10 | 0.121 |
| 7 | 982 | 150±50 | 3.8 | | 40 | 8 | 0.117 |

[a] $D_{col}$: columnar diameter.
[b] $Cr_{cont}$: Cr concentration at bulk state.
[c] $d_{surf}$: thickness oxidized layer.

### 2.4. XPS analyses

The XPS data were obtained by using XSAM-800 (Kratos). A Mg anode with a photon energy of 1254 eV from an X-ray source operating at 15 kV and 20 mA was used for measuring. C 1s, Co $2p_{3/2}$, Cr $2p_{3/2}$ and O 1s spectra were recorded. Binding energies were referenced to the C 1s peak from the contaminated carbon in the surface at 285.0 eV. Basic pressure was below $3 \times 10^{-8}$ Pa.

In order to obtain accurate surface-depth information, we did not perform sputtering. This avoided reduction of the oxide (and/or hydroxide) by ion bombardment (e.g. ref. [19]). Therefore to obtain the depth information of the sample surface, we used ARXPS, by which it is possible to obtain the total depth information from the top of the surface to a certain depth by changing the angles of the samples against the analyser. All the spectra were recorded at photoelectron take-off angles of 20° and 90°.

Every sample was mounted without chemical cleaning.

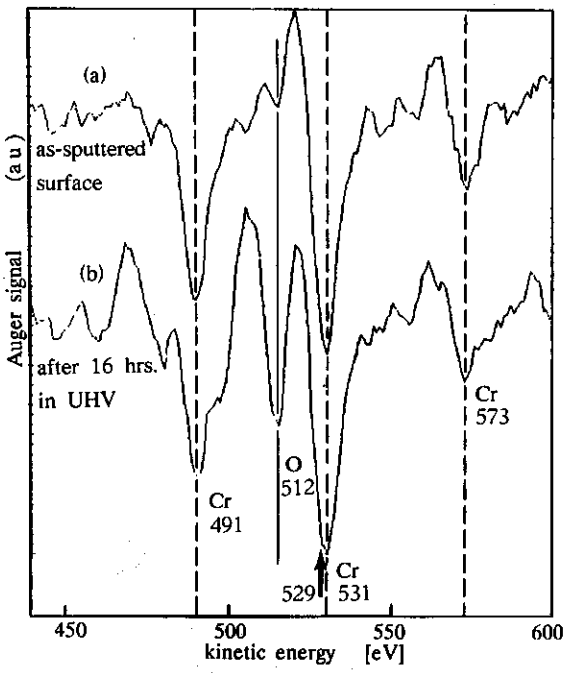


Fig. 1. AES survey scan of Co–Cr sample (no. 7) in the homogeneous area. In (a) the clean-sputtered surface is shown and in (b) the same measurement after storing for 16 h in an UHV.

## 3. Results

### 3.1. Surface chemical state

Oxygen was detected at the surface region of all the samples, which were left as received under ordinary atmospheric conditions for approximately 2 months. After a further 5 months they were again measured. In both cases analysed AES results were found to be the same. It is considered from this result that the stability of the sputtered Co–Cr samples is good.

In order to understand the initial oxidation process we studied the aging effect for the sample in Ultra-High Vacuum (UHV). In fig. 1 the AES signals are given as a function of the kinetic energy. An oxygen-free bulk Co–Cr spectra is shown in fig. 1(a), which was obtained after clean-sputtering for 15 min. The sputtering time can be transformed into the depth values of the samples by using a sputter rate which is nearly the same for Co and Cr [9,10]. In this case it was about 10 Å/min for metallic state Co, Cr and Co–Cr. In fig. 1(b) the same area was again measured after storing the sample in the AES system for 16 h (initial state; $1 \times 10^{-6}$ Pa and after 16 h; $3 \times 10^{-8}$ Pa). A clear oxygen peak, which was not seen in fig. 1(a), can be observed after exposure for 16 h in the UHV state. The double Cr peak (indicated by arrow) suggests that the oxygen is already bounded to the Cr.

Fig. 2(a) shows two different plots of the Cr/Co concentration ratio at the surface region obtained by AES depth profiling on samples nos. 2 and 7. Fig. 2(b) shows the oxygen peak intensities of these samples which were left for 7 months under ordinary atmospheric conditions after deposition. In order to calculate the Cr/Co ratio, we used a Cr peak energy of around 529 eV and for Co one of 775 eV. These energies are the main peaks of the separated three peaks of Auger LMM transitions. However the Cr peak is nearly overlapped by the oxygen peak of 514 eV. Thus if the Cr peak is calculated by the peak-to-peak height, a strong oxygen presence in the surface prevents the cor-

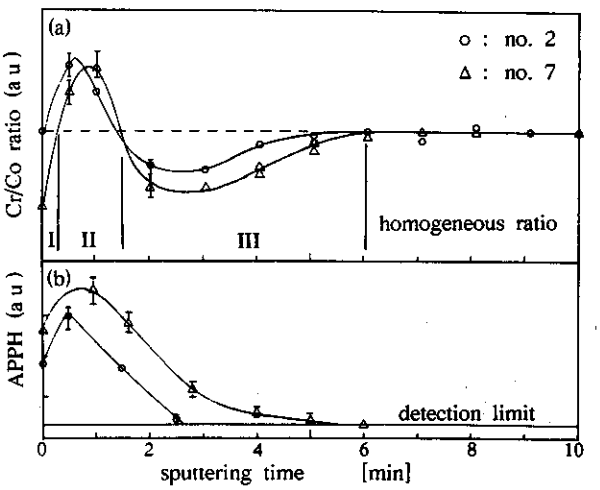


Fig. 2. (a) Peak-to-peak ratio of the Cr 529 eV and the Co 775 eV and (b) the oxygen 514 eV peak intensity as a function of AES sputtering time (samples nos. 2 and 7). APPH: AES peak-to-peak height, sputtering rate: 10 Å/min.

rect estimation of the Cr signal. Hence, for calculating the Cr concentration, a peak-to-background value, which is suggested by Seo and Sato in ref. [20], is used to obtain more accurate qualitative information. Average values were obtained for both plots after 2–4 measurements. At the same time we performed the same measurement on the other samples (nos. 1 and 3–6) and these values have approximately the same fit as those which are drawn in fig. 2(a).

Near the surface (region II in fig. 2(a)), Cr enrichment occurred in every sample, and below this region a Cr-poor (Co enrichment) region (region III in fig. 2(a)) was observed. At the top of the surface (region I in fig. 2(a)) very thin Cr-poor

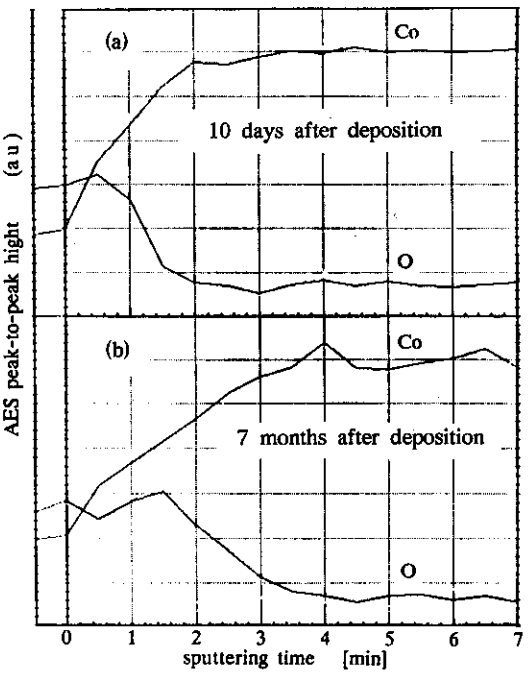


Fig. 3. AES depth profiles of the Co sample. Sputtering rate: 20 Å/min.

(layer) was observed. The oxygen signal reached the detection limit (fig. 2(b)) between at the Cr-poor region for the thinner sample (no. 2) and at the turning point from Co enrichment to the homogeneous ratio for the thicker sample (no. 7). This indicates that the Cr has a tendency to segregate to the surface where it is oxidized (and/or hydroxidized).

We obtained data for fig. 3 from an AES depth profiling study of a pure Co sample. Here the AES

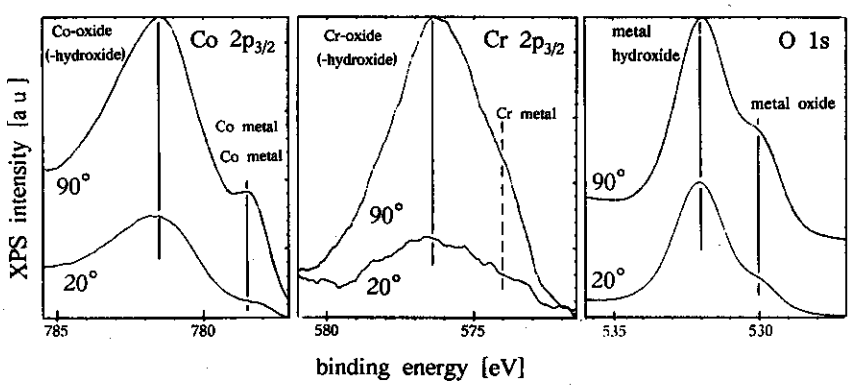


Fig. 4. ARXPS peak spectrum in the Co–Cr sample (no. 3).

intensities of Co and oxygen are given as a function of the kinetic energy. The calculated sputtering rate for metallic Co was about 20 Å/min. Fig. 3(a) was obtained by measuring on an as-received sample which was left under ordinary atmospheric conditions for 10 days. After 7 months it was again measured as shown in fig. 3(b). It can be seen from these figures that the oxygen had penetrated deeper into the sample after 7 months.

In fig. 4 the XPS Co $2p_{3/2}$, Cr $2p_{3/2}$ and O 1s spectra of sample no. 3 were measured by ARXPS. All the binding energies were chosen according to ref. [21] and they were also in agreement with the previous reports [9,12]. Here the XPS intensities are given as a function of the binding energy for angles of 20° and 90°. The information in the signal from the surface depends on the indicated angle. The relative information depth from the surface at 20° is considered to be 1/3 of that at 90°.

At 20° the oxidized Co peak was clearly shown and its chemical state was CoO, while Cr was almost hardly detectable. On the other hand oxygen existed mainly in the hydroxidized state. Thus the top of the surface, a very thin region, is considered to be constructed mainly of hydroxidized Co. At 90° the metallic state of the Co was seen together with the oxidized (and/or hydroxidized) Co but the Cr was in a state of oxide (and/or hydroxide). Further in the oxygen the oxidized state was increased relative to the hydroxidized state. It is quite difficult in both Co and Cr to determine whether the element is oxidized, hydroxidized or both because of the very slight difference of both binding energies (for Co, ref. [21] and Cr, ref. [22]). We could not decide from our data whether the hydroxidized state at the top layer was only $Co(OH)_2$, double salt with oxide and hydroxide, or both.

### *3.2. Surface oxidation as a function of sample thickness*

Fig. 5 is the calculated depth of Cr and $Cr_2O_3$ obtained from the Cr chemical shift in the AES spectra using the method introduced by Okada et al. [23]. The oxide thickness was obtained by comparing the difference in the kinetic energies of the Cr peaks which were split up into three lines of the LMM transition peaks. In this calculation the oxidized Cr was assumed to be only in the form of $Cr_2O_3$. These results were calculated from the difference of the kinetic energies of the Cr peaks and their shifting without paying any atten-

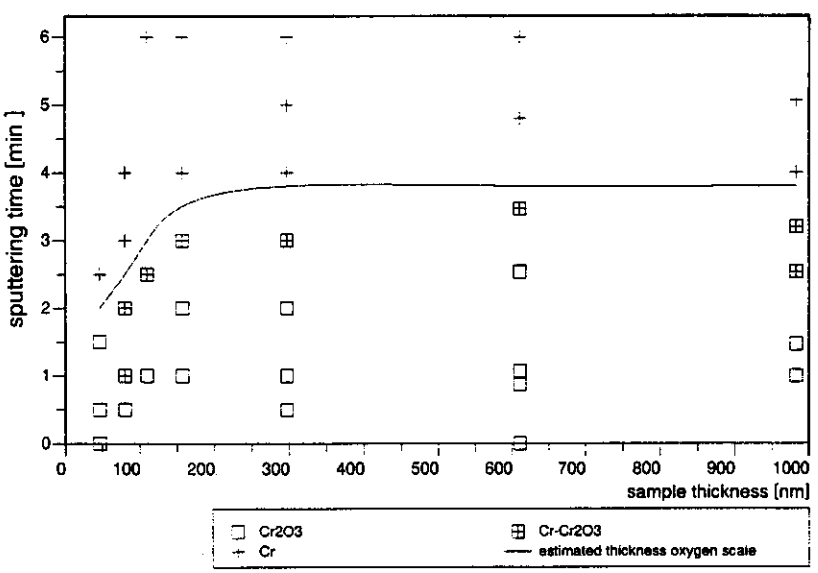


Fig. 5. State of Cr in Co–Cr samples calculated from the shifts in AES spectra as a function of the sample thickness. Sputtering rate: 10 Å/min (as-normalized).

tion to the Co peaks. However, at the interface between the end of the detected oxygen and the metallic state, only the Cr is expected to be oxidized. Therefore it is possible here to neglect the state of Co.

The existence of a both metallic and oxidized Cr was found between the oxidized top layer and the metallic bulk region. The line in fig. 5 describes the estimated thickness of the oxygen scale. As can be seen the thickness of the oxidized area depends slightly on the sample thickness and is constant for samples thicker than 150 nm.

The estimated thickness of the oxidized layer ($d_{surf}$) from fig. 5 is also presented in table 1 together with the magnetic data. In the discussion above we assumed that the sputter rate is constant for all the samples. Calculations on the results of $Ar^+$ ion sputtering experiments from surface to substrate show that this is a reasonable assumption.

## 4. Discussion

### 4.1. Surface chemical state

From the result of the aging effect in UHV, it is considered that the oxidation process develops within a very short period of time (fig. 1). The first oxidation of Cr could be explained by the different free energies of oxidation between Cr to $Cr_2O_3$ and Co to CoO [24]. The concentration ratio of Cr to Co by AES peak-to-peak intensities, after 16 h exposed to UHV (fig. 1(b)) was almost the same as that for the as-sputtered surface (bulk state, fig. 1(a)). The equilibrium dissociation pressure between Co and oxygen is higher than that between Cr and oxygen. And in the UHV state, the pressure becomes closer to the equilibrium dissociation pressure between Co and oxygen than that under ordinary atmospheric conditions. The affinity of Cr towards oxygen is larger than that of Co towards oxygen, therefore it is considered that the preferential oxidation of Cr will occur.

As recognized from fig. 2, a very thin co-rich region is observed which is considered to be oxidized (hydroxidized) regarding the ARXPS results of fig. 4. The assumed escape depths of the information are expected to be 5 and 15 Å for 20° and 90°, respectively. As pointed out in ref. [15], Co cation diffusion in CoO is about 1000-times larger than that of Cr in $Cr_2O_3$, and the diffusion coefficient of oxygen in CoO is also three orders of magnitude lower than that of Co, and that of Cr is three orders of magnitude large than that of oxygen in $Cr_2O_3$ at a high temperature (above 1000 °C). Moreover, the solubility limit of Cr in CoO is only 1 at% at 1000 °C [25]. Therefore it is considered that after the initial oxidation mentioned above, the oxidation process is governed by the selective diffusion of Co to the surface and the Co top layer is formed as a result. The existence of this top layer on the initial oxidized layer is concluded from the results of AES (fig. 2) as well as ARXPS results (fig. 4) and it consists of very thin oxidized (and/or hydroxidized) Co. The XPS pattern in ref. [13], as-annealed at 315 °C for 30 s, shows good agreement with our results. However, in their as-deposited sample, only metallic Co is observed with oxidized Cr. The difference may be considered to be the effect of aging, in other words, the period between the deposition and the analysis.

It can be seen from fig. 3 that the oxidation in the pure Co develops with time. On the other hand no aging effect was observed in the pure Cr sample. This confirms the above-mentioned difference in diffusion coefficients. The oxidized Co–Cr films are also stable over a long period of time. Thus the oxidized Cr is considered to behave as a passive layer in the oxidation process. Accordingly the next three stages can be distinguished in the oxidation process of Co–Cr samples.

- The initial oxidation of the first atom layers.
- Diffusion of the Co mainly through the CoO to the surface. This Co forms the CoO top layer on the top of the $Cr_2O_3$ (Co-depleted) layer.
- A $Cr_2O_3$ layer acts as a passive layer which prevents the films from further oxidation.

Following ref. [19], we searched for the existence of $Co_3O_4$ in ARXPS. However, under our experimental conditions, it is almost impossible to distinguish the peak-binding energy of $Co_3O_4$ from that of CoO as well as from that of $CoCr_2O_4$ with

a spinel structure which was observed at high temperature annealing [14–16].

From fig. 4 the surface state is considered to be mainly hydroxidized. The hydroxidized surface was reported in ref. [10]. They analysed the sputter-cleaned surface after it had been left for about 20 min under ordinary atmospheric conditions. It was observed that the surface states of the Co and Cr were mainly hydroxidized, but about 25% of the Co and Cr still remained in the metallic states. It can also be seen in ref. [12] that the metallic states of Co and Cr were 8.5 and 1.4 at% respectively after 2 days exposure to the ordinary atmospheric conditions. The initial change of the surface may be attributed to be the absorption of water from the atmosphere. However, from all the above results the surface hydroxidation occurs within a very short time. It can be concluded that our result has a similar tendency to the one mentioned above, although the specimen was stored under ordinary atmospheric conditions for much longer. Therefore we arrive at the conclusion that under ordinary atmospheric conditions, the top layer of a Co–Cr sample is considered to be mainly dominated by the hydroxidized species.

### 4.2. Four-layered structure model

Although there are several different conditions, the same tendency in our results for the layered model can be deduced from previous reports [7,8,13]. In ref. [7] the Co-depleted region near the surface and Co-rich top layer are also observed. This result was obtained by annealing for about 10 min at 500 °C in $10^{-3}$ Torr. In ref. [8] they suggest the double-layered structure, which is obtained by annealing at 400 °C. Also in ref. [13], they observe a three-layered-like structure. Only the result of Swami and Haines [9] is different. They observe that the surface of every sample is dominated by oxidized Cr in spite of different annealing conditions including as-sputtered samples. Fowler and Rogozik pointed out in ref. [10] that this difference originates from the higher Cr concentration. However our Cr concentration is almost the same (19.2 at%) as that of ref. [9], but

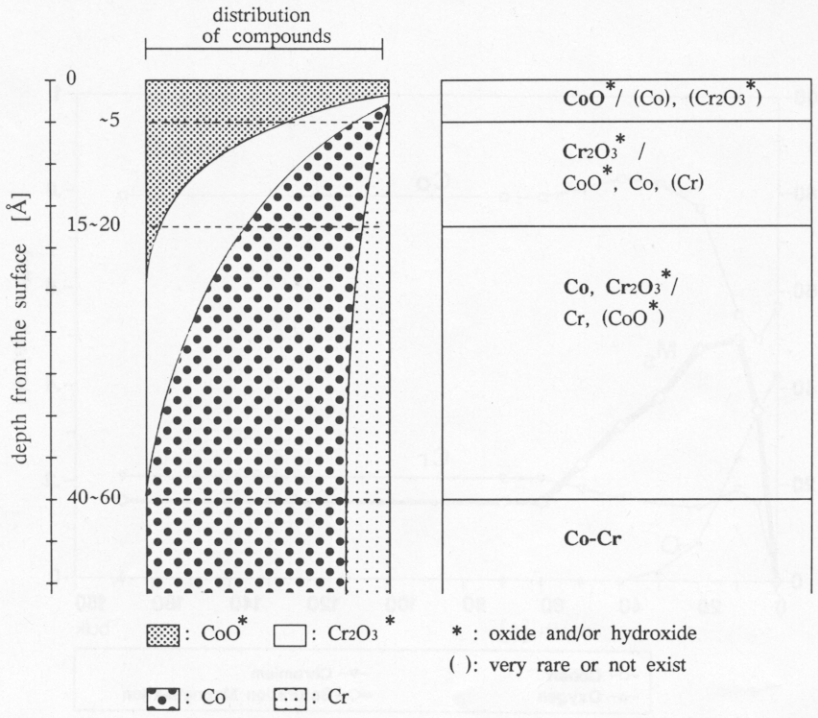


Fig. 6. Schematic four-layered structure model of the cross-section of the Co–Cr sample (right side) and a qualitative distribution of the compounds in the surface (left side).

our samples show the surface concentration of the oxidized Co. The only plausible explanation is the formation of the pure $Cr_2O_3$ layer in the top layer under certain circumstances, which may prevent the diffusion of Co to the surface. For example, annealing in UHV may cause the oxidized Cr layer that is presumed from the results of fig. 1.

Oxygen was observed throughout the regions where the Cr/Co ratio is different from that of the bulk region. Therefore, if the Cr/Co ratio of the sample differs from the bulk ratio, the Cr and a part of the Co will be oxidized.

Summarising these statements we suggest that the oxygen scale on our rf sputtered Co–Cr samples can be described by the four-layered structure model in fig. 6. On the right side a cross-section of the different observable layers is shown. The left part of the figure shows a qualitative distribution of the compounds through the film. As can be seen from this figure, the surface contains only CoO. Below this region $Cr_2O_3$ enrichment occurs. At around 50 Å from the surface only metallic (bulk concentration) Co–Cr is observed.

### 4.3. Thickness dependence

From the results in fig. 5 we conclude that there is no essential difference in the surface oxidation mechanism of the samples with sample thickness. Further, the thickness of the oxidized region is limited.

As clarified above, the treatment of the samples during the period between the deposition and analysis can have a great impact on the formed oxygen scale. Because our samples are deposited on a water-cooled substrate the substrate temperature will increase during the first 900 s of our deposition process by about 200 °C. Therefore the first annealing process, occurring during deposition, takes place at a lower temperature for the thinner films.

Another possible reason of the observed thick-

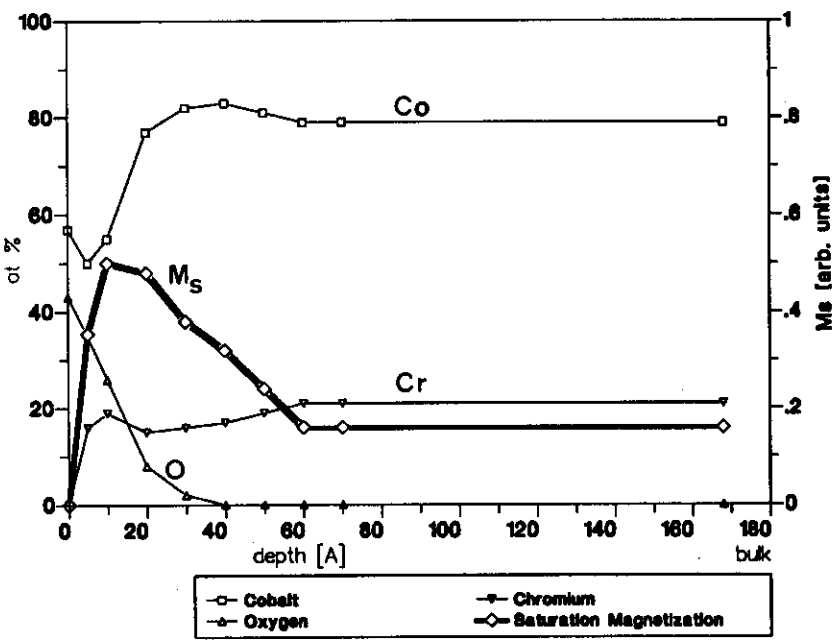


Fig. 7. Relation between chemical composition and calculated saturation magnetization in Co–Cr sample (no. 7). Sputtering rate: 10 Å/min.

ness dependence could be the surface roughness. If the columnar size is largely increased for the thicker films the roughness of the surface is also more pronounced (see table 1 for columnar size).

### 4.4. Correlation between chemical composition and magnetic parameters

In table 1 the most important magnetic parameters are presented together with the thickness of the oxygen scale for the samples studied. Although $d_{surf}$ is thickness-dependent like most of the magnetic data presented, any conclusion about a causal relation would be premature at this stage of research.

In fig. 7 we plot the at% Cr, Co and oxygen as a function of the distance to the surface of sample no. 7 using the results of AES survey scanning throughout the film. As shown in ARXPS measurements, no Cr exists at the surface of the film. Therefore the Cr concentration at the surface is assumed to be 0 at% in fig. 7. The saturation magnetization was calculated from the chemical data under the following assumptions:

- Oxygen will react with Cr to form $Cr_2O_3$ (non-ferromagnetic).
- If any oxygen is left this will dilute the Co and decrease $M_S$.
- If all the oxygen is bounded to Cr, the unbounded Cr will dilute the Co and decrease $M_S$.
- For the influence of oxygen and Cr on the $M_S$ of Co we used the linear relations [26,27]:

$$M_S = \mathrm{mol}_{(Co)} - 2 \times \mathrm{mol}_{(O)}, \quad M_S > 0,$$

$$M_S = \mathrm{mol}_{(Co)} - 3 \times \mathrm{mol}_{(Cr)}, \quad M_S > 0,$$

where:

$M_S$: the saturation magnetization (arbitrary unit),

$\mathrm{mol}_{(O)}$: the number of oxygen atoms,

$\mathrm{mol}_{(Co)}$: the number of cobalt atoms,

$\mathrm{mol}_{(Cr)}$: the number of chromium atoms.

As can be seen from fig. 7, these calculations suggest the existence of a region with enhanced saturation magnetization just under the top layer. The presence of an oxygen layer will change the charge distribution in the system and in this way influence the magnetic reversal mechanism in the sample. Note that the penetration depth of light is about 15 nm ($\lambda = 632.8$ nm), which is three times larger than the thickness of the oxygen layer. Therefore it will be clear that the measured MO properties can be largely different from those of the bulk material. Annealing experiments in air and MO measurements at other wavelengths (i.e. other penetration depth) could give us quantitative information about the influence of the quadruple oxygen scale on the magnetic parameters.

## Acknowledgements

The authors would like to thank A.H.J. van den Berg for his helpful assistance with AES and XPS measurements. They also wish to express appreciation to Dr. L.J. Hanekamp and Dr. E.M.C.M. Reuvekamp for their fruitful discussions about AES data. Thanks are also due to J. Baxter for his cooperation and Prof. Dr. Th. J.A. Popma for his continuous support. This research is partly supported by the Community Action on Magnetic Storage Technology (CAMST).

## References

[1] K. Ouchi, J. Magn. Soc. Jpn. 13-Suppl. S1 (1989) 611.
[2] M. Abe, K. Shono, K. Kobayashi, M. Gomi and S. Nomura, Jpn. J. Appl. Phys. 21 (1982) L22.
[3] K. Tsutsumi, Y. Fujii, M. Komori, T. Numata and Y. Sakurai, IEEE Trans. Magn. MAG-19 (1983) 1760.
[4] J.W. Smits, S.B. Luitjens and R.W.J. Geuskens, IEEE Trans. Magn. MAG-20 (1984) 60.
[5] K. Hemmes, W. Lisowski, J.C. Lodder, L.J. Hanekamp and Th.J.A. Popma, J. Phys. D 19 (1986) 1311.
[6] W.J.M.A. Geerts, J.G.Th. te Lintelo, J.C. Lodder and Th.J.A. Popma, IEEE Trans. Magn. MAG-26 (1990) 36.
[7] J.W. Smits, S.B. Luitjens and F.J.A. den Broeder, J. Appl. Phys. 55 (1984) 260.
[8] S. Honda, N. Yamashita, M. Ohkoshi and T. Kusuda, IEEE Trans. Magn. MAG-20 (1984) 791.
[9] G.T.K. Swami and W.G. Haines, Appl. Surface Sci. 21 (1985) 151.
[10] D.E. Fowler and J. Rogozik, J. Vac. Sci. Technol. A 6 (1988) 928.
[11] K. Honda, R. Sugita, N. Echigo and Y. Sakamoto, IEEE Trans. Magn. MAG-24 (1988) 2664.
[12] V. Novotny and N. Staud, J. Electrochem. Soc. 35 (1988) 2931.

[13] O. Kitakami, Y. Ogawa, S. Yamagata, H. Daimon and T. Maro, IEEE Trans. Magn. MAG-26 (1990) 2676.
[14] P.K. Kofstad and A.Z. Hed, J. Electrochem. Soc. 116 (1969) 224.
[15] P.K. Kofstad and A.Z. Hed, J. Electrochem. Soc. 116 (1969) 229.
[16] P.K. Kofstad and A.Z. Hed, J. Electrochem. Soc. 116 (1969) 1543.
[17] J.C. Lodder and T. Wielinga, IEEE Trans. Magn. MAG-20 (1984) 57.
[18] W.J.M.A. Geerts et al., to be published.
[19] T.J. Chuang, C.R. Brundle and D.W. Rice, Surface Sci. 59 (1976) 413.
[20] M. Seo and N. Sato, Trans. JIM 21 (1980) 805.
[21] C.D. Wagner, W.M. Riggs, L.E. Davis and J.F. Moulder, Handbook of X-ray Photoelectron Spectroscopy (Perkin–Elmer, Eden Prairie, MN, 1979).
[22] E. Desimoni, C. Malitesta, P.G. Zambonin and J.C. Rivière, Surface Interface Anal. 13 (1988) 173.
[23] H. Okada, H. Ogawa and H. Omata, Hyomen (Surface) 12 (1974) 148 (in Japanese).
[24] D.R. Gaskell, Introduction to Metallurgical Thermodynamics (McGraw-Hill Kogakusha, Tokyo, 1973).
[25] J. Nowotny, I. Sikora and J.B. Wagner, J. Am. Ceram. Soc. 65 (1982) 192.
[26] N. Hiratsuka, M. Moteki, S. Kobayashi, T. Namikawa and M. Sugimoto, Trans. IECE Jpn. J72-C (1989) 237 (in Japanese).
[27] W.G. Haines, J. Appl. Phys. 55 (1984) 2263.